ACS APPLIED NANO MATERIALS

www.acsanm.org Article

Resistive-Pulse Nanopore Sensing of Ligand Exchange at the Single Nanocluster Limit for Peptide Detection

Bobby D. Cox, Madhav L. Ghimire, Massimo F. Bertino, and Joseph E. Reiner*

Cite This: *ACS Appl. Nano Mater.* 2020, 3, 7973–7981 Read Online

ACCESS | Metrics & More | Article Recommendations | Supporting Information

ABSTRACT: Water-soluble metallic nanoclusters require passivating ligands to stabilize and, in many cases, derivatize their surfaces. Recently, we demonstrated the use of resistive-pulse nanopore sensing to observe ligand-induced structural fluctuations of individually trapped nanoclusters. Here we expand on this capability by observing real-time ligand exchange at the single cluster limit. The nanopore technique allows time-resolved observations of ligand exchange and ligand addition with exchange times that agree with calculated free energy profiles. The observed kinetics for thiolated poly(ethylene glycol) (S-PEG) ligands exchanging with tiopronin and glutathione-capped gold clusters is on the order of seconds within the nanoconfined region of the pore, and this rapid exchange motivates the development of a new peptide sensor. We also show proof of concept that nanopore-based exchange between a peptide target (glutathione) and a tiopronin-capped gold cluster leads to current fluctuations that enable identification of the peptide.

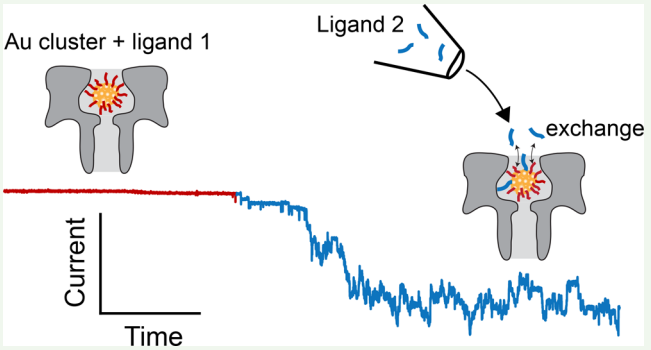

KEYWORDS: *nanoclusters, nanopore, peptide, ligand exchange, glutathione*

1. INTRODUCTION

Water-soluble metallic nanoclusters have many applications that include medical imaging,[1] virus detection,[2] immunosensors,[3] and drug delivery.[4] In most cases, optimizing clusters for these applications requires enhancing the interaction between the clusters and a target. One of the most common approaches to do this is to synthesize clusters that are passivated with ligands designed for specific interactions. Usually this requires synthesizing clusters with one type of ligand followed by a ligand exchange step.[5−8] Ligand exchange is typically performed by adding an excess of free ligands of the desired type to a suspension of passivated clusters. Over time (minutes to hours[5,9−13]) the target ligands exchange with the cluster-passivating ligands, and this creates clusters with the desired surface characteristics. Numerous studies have looked at this process to better understand the parameters affecting exchange kinetics.[14−17] The majority of ligand exchange characterization has utilized bulk or ensemble-based methods (i.e., NMR, IR spectroscopy, and chromatography).[18,19] However, monitoring individual clusters undergoing exchange in real time would provide a better understanding of the many variables involved in the exchange process (i.e., ligand size, functional group, ligand flexibility, etc.).

Our previous study utilizing resistive-pulse nanopore sensing for cluster characterization provides the starting point for studying ligand exchange at the single cluster limit.[20] The principle of operation for nanopore sensing is based on the Coulter counter applied at the nanoscale,[21] and many reviews on the subject of nanopore sensing have already been written.[22−28] Nanopore sensing for nanoparticle characterization has grown over the past few years to include characterization of MPSA-capped gold clusters,[29] heteropolytungstates,[30] and glutathione-capped gold clusters.[31] A thorough review on the use of nanopore sensing for studying nanoclusters can be found elsewhere.[32] In our previous work, we showed that metallic clusters with a diameter of ca. 2 nm can be trapped for minutes inside an α-hemolysin (α-HL) pore. These long trapping times allow one to monitor cluster structure fluctuations for extended periods.[20] The ability to simultaneously trap and probe an individual cluster in real time is not accessible to other analysis techniques and is unique to the nanopore sensor.

In this paper we extend our previous work, which utilized the pore's ability to trap small metallic clusters, to investigate both homogeneous ligand exchange (where the exchanged ligand is identical to the ligand being replaced) and heterogeneous exchange (where the exchanged ligand is

Received: May 27, 2020
Accepted: July 21, 2020
Published: July 21, 2020

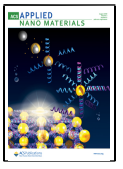

different from the ligand being replaced). Analysis shows that nanopore sensing enables time-resolved measurements of both exchange kinetics and efficiency on a single cluster's surface. This provides a new means for testing the efficacy of ligand exchange, showing that nanopore sensing provides a rapid means for optimizing cluster surfaces via ligand exchange.

In addition to utilizing the nanopore sensor for characterizing ligand exchange, we also demonstrate that the exchange process could enable a new approach to single molecule peptide sensing. There is growing interest in utilizing nanopores for peptide detection[33−35] in part because of the burgeoning field of nanopore-based DNA sequencing[36] and because nanopore sensing could provide rapid and low-cost early screening for cancer.[37,38] Here we show that our methodology provides an alternative route to peptide sensing where a trapped cluster serves as the transducer that initiates unique current fluctuations in response to peptide exchange. The results illustrate a new path toward small molecular weight peptide detection where the clusters (and not the pore[39]) could be modified to enhance peptide detection.

2. RESULTS

Resistive-pulse nanopore sensing enables the isolation and capture of individual metallic clusters for extended periods (ca. 10^2 s), allowing one to investigate ligand-capped clusters in the presence of freely diffusing ligands. Figure 1A shows the experimental setup for the two-tip exchange protocol used throughout most of this article. Single-tip protocols are also possible, as shown in Figure S1 (see the Supporting Information) for S-PEG$_7$ homogeneous exchange. Observation of ligand exchange on a single, isolated cluster is highlighted in Figure 1B, which shows a sample current trace of an exchange experiment. The ability to isolate a single cluster allows for the unique demonstration of ligand interactions with clusters passivated with the same ligand as the freely diffusing ligands via so-called homogeneous ligand exchange.

2.1. Homogeneous Exchange. Homogeneous exchange using the two-tip and one-tip approach is demonstrated in Figure 2 for S-PEG$_7$ and TP (tiopronin)-capped gold clusters. In both cases, we find a strong dependence of cluster-structure fluctuation kinetics on free ligand concentration. Figure 2A shows the case for S-PEG$_7$ ligands. Prior to capture of a cluster, short current blockades can be seen corresponding to interactions between the pore and free S-PEG$_7$ originating from excess ligand left over from the synthesis. Upon capture of the cluster, the current decreases by about a factor of 3. Fluid from the particle tip continues to eject for a short time as the particle fluctuates through discrete current steps corresponding to ligand-induced changes in the cluster structure. After ca. 5 s (from the start of the trace) the pump is turned off, which results in a lack of excess ligand around the pore region (confirmed by the absence of short current blockades upon exit of the cluster from the pore). Figure 2A shows a reduction in the fluctuation rate of the cluster with the removal of excess ligand in solution. We hypothesize that this shows free ligands in the vicinity of the particle yield either self-exchange (i.e., a freely diffusing PEG exchanges with a surface bound PEG) or nonexchange interactions with the ligand shell. We note that the overall current level (≈50 pA) is unaffected in the presence of the freely diffusing PEG ligands, and the current steps for the S-PEG$_7$ process are resolvable before and after the fluid is turned off. Further analysis on the corresponding current fluctuations that includes current

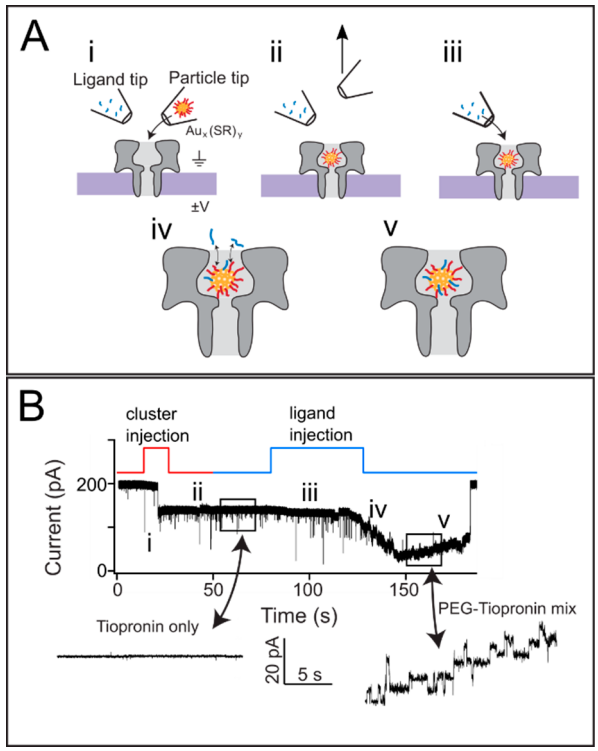

Figure 1. Nanopore-based two-tip exchange protocol and corresponding current trace. (A) One tip injects single metallic clusters into the pore while a second pipet tip injects different ligands in the vicinity of the cluster-occupied pore. The protocol consists of five steps: (i) Solution from a tip containing particles is ejected onto the pore until a single particle is captured. (ii) To ensure no further particles enter the pore, the particle tip is removed. (iii) After a short delay (∼1 min) the second ligand is ejected onto the trapped particle. (iv) The freely diffusing ligand interacts with the trapped particle. (v) The postexchange particle is monitored. (B) A typical experiment with the five steps highlighted. In this case, a TP-capped gold cluster is trapped and exposed to S-PEG$_7$ ligands. The red trace above the data corresponds to the cluster tip pressure, and the blue trace illustrates the secondary ligand tip pressure. The two rectangular boxes on the raw data are highlighted with 100 Hz low pass filtering. Data in (B) were collected in 3 M KCl at pH 8 under a 70 mV applied transmembrane potential. The S-PEG$_7$ concentration in the ligand tip was 200 μM.

histograms, corresponding current state peak positions, and step fluctuation kinetics can be found in Figure S2. These results show that the magnitude of the current steps seen in Figure 2A are consistent with our previously reported values.[20] Kinetic analysis of the stepwise fluctuations (Figure S2D) shows the current step-time distributions before and after the excess ligand source is turned off. These fluctuations show an ∼3.5-fold increase in the step time when the fluid is turned off. This suggests that the freely diffusing PEG affects the structure fluctuations of the trapped cluster, but the size of the cluster remains the same and thus no net exchange occurs.

To further investigate homogeneous exchange, we performed an experiment on TP-capped clusters (Figure 2B and Figure S2E−H). For the case of TP homogeneous exchange, we found no evidence of excess TP ligands in the particle loading tip (i.e., most of the TP ligands were bound to cluster surfaces), so we collected this data using the two-tip protocol from Figure 1A. Upon capture of a TP-capped cluster, the current was monitored for ca. 60 s before ejecting free TP

https://dx.doi.org/10.1021/acsanm.0c01451
ACS Appl. Nano Mater. 2020, 3, 7973−7981

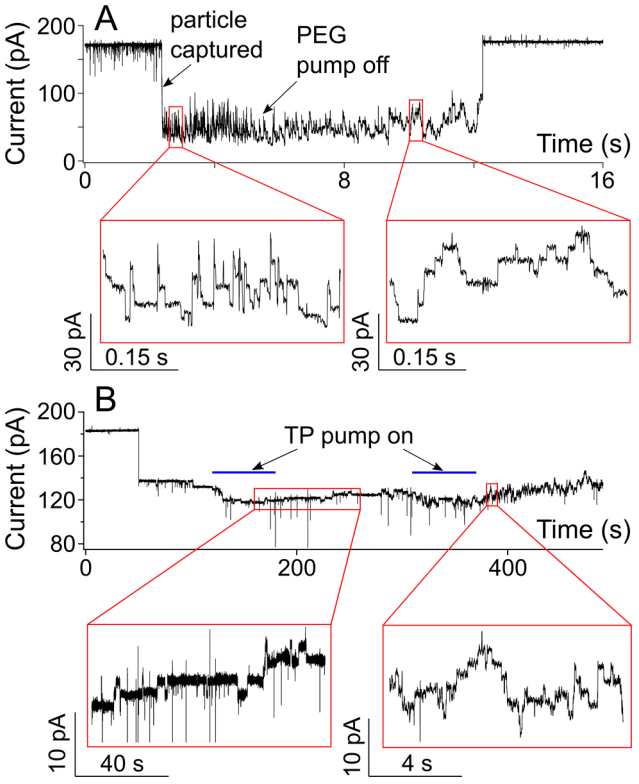

Figure 2. Homogeneous exchange for S-PEG$_7$ and TP-capped gold clusters. (A) Full current trace of an S-PEG$_7$-capped gold cluster captured by the pore. At t = 5.5 s, the freely diffusing S-PEG$_7$ ligands are removed, and the current fluctuations change. The red boxes highlight discrete current steps before and after the excess ligands are removed. After the pump is turned off, the steps remain but are slower. (B) TP-capped clusters exposed to free TP ligands. As with the S-PEG$_7$ example, the fluctuation kinetics change after the free ligands are removed. The S-PEG$_7$ data were filtered with a 1 kHz filter while the TP data were filtered with a 100 Hz filter. Data were collected in 3 M KCl at pH 8 under a 70 mV applied transmembrane potential. The S-PEG$_7$ and TP tips contained 22 and 165 μM of free ligand, respectively. A complete analysis of the corresponding fluctuations can be found in Figure S2.

ligand solution onto the cluster from a tip containing 165 μM of free TP ligands. The excess ligands resulted in a striking change in current fluctuations that suggest TP-capped clusters are capable of either rapid homogeneous exchange or addition of excess ligands onto the trapped cluster. The addition of excess ligands may be due to a shift in equilibrium toward the cluster bound state within the pore environment due to the presence of a single cluster and excess freely diffusing ligand molecules.

We believe the former is the more likely case given the stable nature of the current prior to free ligand ejection. Regardless, the TP-capped cluster fluctuations continue after each free ligand ejection. This suggests that the TP cluster undergoes a lasting change because the resulting fluctuation kinetics remain well beyond the time one would expect the freely diffusing TP ligands to diffuse away from the particle (<1 μs). This motivates our hypothesis that at least in the case of TP−TP homogeneous exchange the process leads to an irreversible change in the cluster's structure and fluctuation kinetics. We hypothesize that this results from ligands detaching and reattaching in random locations and orientations on the cluster surface. Further study is required to better understand this phenomenon, which is beyond the scope of the present paper.

2.2. Heterogeneous Exchange. After completing the homogeneous exchange experiments, we investigated heterogeneous ligand exchange for TP- and glutathione (GT)-capped clusters in the presence of freely diffusing S-PEG$_7$ and S-PEG$_4$ ligands. The current traces in Figure 3A and Figure S3 show

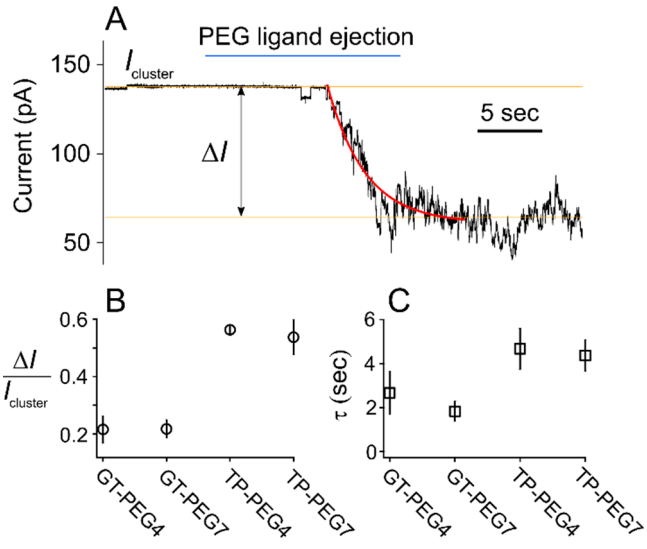

Figure 3. Heterogeneous ligand exchange. (A) A TP-capped particle is trapped in the pore and yields a steady current ($I_{cluster}$ = 137.6 pA). S-PEG$_4$ ligands are ejected onto the particle over a 20 s period (ligand exposure time is indicated by the solid blue line). This leads to a rapid decrease in the current to a new level ($I_{cluster} - \Delta I$ = 64.2 pA). To extract the exchange rate (τ), we perform a least-squares fit with an offset exponential ($i(t) = i_0 \exp(-(t - t_0)/\tau)$) (solid red line) and find τ = 2.9 ± 0.1 s. (B) S-PEG$_4$ and S-PEG$_7$ exchange was performed with TP and GT-capped clusters. (C) Average exchange times (corrected for exchange tip analyte concentrations) are on the order of seconds for each condition. Each data point in (B) and (C) corresponds to a minimum of four different exchange experiments. Error bars correspond to ±1 SE. All data were taken in 3 M KCl at pH 8.0 with an applied transmembrane potential of 70 mV. The S-PEG concentration in each tip was 540 μM, except for the TP-PEG$_7$ experiments where [S-PEG$_7$] = 200 μM.

the trapped cluster exposed to extended periods of free unbound ligands via ejection from the so-called ligand tip. In each case the current shows discrete downward steps indicating exchange between the passivating layer and the freely diffusing ligands. The cluster modification occurs over a period of seconds, and the degree to which the current (cluster structure) changes in the presence of the thiolated-PEG injection depends mostly on the capping ligand of the trapped gold cluster.

Analysis of the exchange process leads to several conclusions regarding the particle modification and exchange time. Figure 3A shows how we quantify the exchange time τ (i.e., the decay time of the current as it goes from the preligand ejection value ($I_{cluster}$) to the postligand ejection value ($I_{cluster} - \Delta I$)) and the overall change in current ΔI. These parameters are related to the change in cluster size and exchange efficiency. Full current traces for each type of exchange experiment are reported in Figure S3. Figures 3B and 3C highlight differences and similarities in these parameters among the four examples studied. We find several noteworthy results. First, Figure 3B

https://dx.doi.org/10.1021/acsanm.0c01451
ACS Appl. Nano Mater. 2020, 3, 7973−7981

shows that freely diffusing thiolated PEG leads to greater changes in the overall current for TP-capped clusters than for GT-capped clusters, which suggests that TP-capped particles are more susceptible to PEG exchange than GT-capped particles. We hypothesize that the mechanism for this is related to steric hindrance because the larger glutathione ligands preclude exchange, but further studies are required to address this more fully. Second, the change in current is comparable for S-PEG_4 and S-PEG_7. This is surprising because one would expect the larger PEG (S-PEG_7) to create a greater change in the current, but this could be explained if either the exchange efficiency (i.e., the percentage of ligands replaced during the exchange process) or the rate of exchange (i.e., $1/\tau$) is greater for S-PEG_4 than S-PEG_7. Figure 3C shows similar exchange rates between each of the conditions reported; thus, it seems more likely that exchange efficiency could explain the results in Figure 3B. We will discuss this in greater detail in subsection 2.4. In any case, all four examples shown in Figure 3 illustrate that the rate of exchange appears to be faster (i.e., ~1 s) than suggested by previous reports (i.e., several minutes to hours[5,9−13]). This may result from the fact that the nanopore isolates individual clusters and thus removes the possibility of long-time kinetics from cluster−cluster interactions.

2.3. Exchange vs Addition. Another benefit to nanopore-based single cluster analysis is the ability to probe individual current (structure) fluctuations both during and after the freely diffusing unbounded ligands are introduced. This enables the isolation of individual ligand interaction events that can be used to quantify the kinetics of single ligand exchange processes. Figure 4 demonstrates this capability by highlighting two distinct current fluctuation types that result from heterogeneous exchange conditions. The first fluctuation type is shown in Figure 4A, and a zoomed-in view is highlighted in Figure 4B. The data show a two-step fluctuation characterized by a large downward step followed by a smaller upward step. The time between these steps is termed the individual ligand exchange time (t_{ile}), and Figure 4C shows that the t_{ile} distribution follows a single exponential with mean individual ligand exchange time for the S-PEG-TP exchange process of (τ_{ile} = 90 ± 20 ms). The illustrations in the top portion of Figure 4B show our interpretation of this fluctuation. A particle is capped with one type of ligand (i.e., black = TP) and exposed to a second freely diffusing ligand (i.e., red = S-PEG). The binding event leads to an increase in the particle size and a downward step in current followed by the release of a TP ligand from the particle and a corresponding upward step in current.

To ascertain the validity of this interpretation of the exchange-induced fluctuation, we note that Fernando and Aikens previously reported calculated free energy landscapes of $Au_{25}(SR)_{18}$ clusters under exchange. There it was found that the energy barriers to ligand detachment following attachment of a freely diffusing ligand are on the order of 0.5 eV.[17] Our results are consistent with these calculations, and this can be seen by connecting the ligand exchange time kinetics to the free energy barrier via Arrhenius rate theory ($\tau = \tau_0 \exp(\Delta G_{off}/k_BT)$). We estimate the prefactor (τ_0) to be the time it takes a TP ligand to diffuse two cluster diameters away from the cluster ($\tau_0 = r^2/6D$, r = 4 nm). We further estimate the TP diffusion coefficient from the Stokes−Einstein equation ($D = k_BT/6\pi\eta a$) where k_B is Boltzmann's constant, T is the absolute temperature (T = 297 ± 2 K), η is the dynamic viscosity of water at room temperature ($\eta = 8.9 \times 10^{-4}$ Pa·s), and a is the

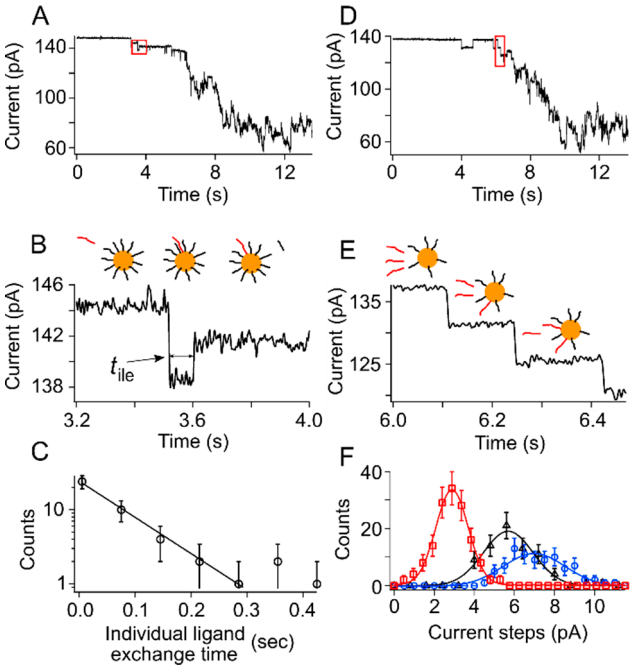

Figure 4. Ligand exchange and ligand addition observed at the single molecule limit. (A) Current trace of S-PEG_4 exchanging with TP-capped gold shows evidence of the two-step exchange process. The red box in the trace highlights a single exchange step. (B) A zoomed-in view of the exchange step. The cartoon illustrates our hypothesized exchange process where an S-PEG_4 ligand binds to the particle and then a smaller TP ligand is released. (C) Least-squares fit to the individual ligand exchange time distribution with a single-exponential function yields the mean individual ligand exchange time τ_{ile} = 90 ± 20 ms (±1 SD). (D) A different current trace of S-PEG_4-TP exchange shows evidence of ligand addition. (E) The zoomed-in region of the red box in (D) illustrates the downward current steps that we hypothesize originate from ligands binding to the cluster with no follow-up detachments. (F) Current step distributions clearly separate the different step sizes. The TP (red squares), S-PEG_4 (black triangles), and S-PEG_7 (blue circles) show peaks located at 2.9 ± 0.1, 5.6 ± 0.2, and 7.0 ± 0.2 pA, respectively (±1 SE), which are consistent with the expected current steps for these ligands.[20] The current was collected in 3 M KCl under a 70 mV applied transmembrane potential.

hydrodynamic radius of a TP ligand (a = 0.35 ± 0.05 nm).[40] This leads to an Arrhenius prefactor of τ_0 = 3.8 ± 0.5 ns. Substituting this prefactor and the experimental mean individual exchange time (τ_{ile} = 90 ± 20 ms) into the Arrhenius equation, we find a free energy barrier to ligand disassociation of ΔG_{off} = 0.43 ± 0.01 eV, which is in very good agreement with the calculated free energy barrier to ligand exchange. This suggests that in spite of the fact that the nanoconfined region within the cluster-occupied pore may introduce effects not present in the bulk[20] (i.e., interfacial water structuring), the nanopore provides a reasonable means of estimating ligand disassociation kinetics.

The second fluctuation of interest is highlighted in Figures 4D and 4E, and it shows consecutive downward steps in the current. We hypothesize that this fluctuation results from ligands attaching to the cluster with no follow-up detachment. This is highlighted by the illustrations above Figure 4E where each downward step corresponds to an additional ligand attaching to the cluster. We hypothesize that these fluctuations most likely result from clusters that have several vacant

https://dx.doi.org/10.1021/acsanm.0c01451
ACS Appl. Nano Mater. 2020, 3, 7973−7981

attachment sites[41] amenable to direct attachment, and this leads to the direct association steps shown here.

To further verify our hypothesis connecting the two current fluctuation types to exchange and addition processes, we performed separate TP-PEG exchange experiments with S-PEG_4 and S-PEG_7. We calculated current step distributions from the current as it changed from the pre-exchange current state (i.e., $I_{cluster}$ in Figure 3A) to the postexchange current state (i.e., $I_{cluster} - \Delta I$ in Figure 3A). Figure 4F shows the current step distributions with three distinct peaks that correspond to TP, S-PEG_4, and S-PEG_7. From these experiments we found that the percentage of exchange-type events (i.e., Figure 4B) for S-PEG_4-TP was 45 ± 7% measured from 13 particle captures distributed over two different pores. Exchange events for S-PEG_7-TP were found to be 31 ± 6% measured from eight particle captures distributed over two different pores. The larger percentage of exchange events for S-PEG_4 vs S-PEG_7 suggests that the overall efficiency of exchange is higher for PEG_4 than PEG_7. This is not completely surprising, given the larger molecular weight of S-PEG_7 most likely results in a greater number of configurations precluding binding to the particle surface. To further explore this possibility, we studied the captured particle's fluctuations following exchange.

2.4. Postexchange Fluctuation Analysis. In addition to monitoring the exchange process, we can also analyze the cluster following exchange. Figures 5A and 5D show typical current traces of a TP-capped particle, exchanged with S-PEG_4 and S-PEG_7, respectively. In both cases, the TP-capped particle remains trapped for an extended period in the pore before the PEG-ligand solution is ejected onto the pore. In the presence of the thiolated PEG, both traces show that the particles undergo a rapid change as evidenced by the raw current trace with corresponding fluctuations. This is shown in Figure 3 and Figure S3, but here we probe the fluctuations following exchange more closely. Figures 5B and 5E show all points histograms for the current following exchange (highlighted by orange boxes in Figures 5A and 5D). Although both distributions yield clearly resolved current states, the peaks from the S-PEG_4 exchange (Figure 5B) can be fit by single Gaussian functions. This contrasts with the S-PEG_7 exchange (Figure 5E) where each peak requires multiple Gaussian functions, indicating multiple substates. To better understand the origin of this difference, we computed current step distributions using a CUSUM algorithm state finder.[42] Figures 5C and 5F show the distributions of the current steps for each case, and these show clear differences between the fluctuations for the S-PEG_4 and S-PEG_7 experiments. Specifically, the S-PEG_4 shows a single peak in the current steps in both positive and negative directions, which suggests complete exchange between S-PEG_4 and the TP-capped gold. In contrast, the S-PEG_7 distribution shows two current step magnitudes. Multipeak fitting analysis shows that the magnitude of the steps for S-PEG_4 are consistent with the expected values for S-PEG_4 only capped particles, while the multiple steps in the S-PEG_7 exposed particles are consistent with S-PEG_7 sized steps and TP sized steps.[20] The averaged area of the peaks in the S-PEG_7-TP exchange distributions are $A_{S\text{-}PEG7}$ = 26 ± 4 pA and A_{TP} = 43 ± 11 pA, which can be translated into an overall exchange efficiency of $A_{S\text{-}PEG7}/(A_{TP} + A_{S\text{-}PEG7})$ = 0.38 ± 0.09. This suggests that the S-PEG_4 ligands yield a more complete exchange with the TP-capped particle while the S-PEG_7 ligands only partially replace the TP-capping ligands. This speaks to the efficiency of exchange, and in this case the S-PEG_4 exchange appears more efficient than S-PEG_7 as suggested by the data and discussion of Figure 3. Overall, this supports the notion that the nanopore fluctuations can be used to characterize the ligand exchange kinetics, within the pore, at the single ligand limit, and they can also be used to quantify the exchange efficiency.

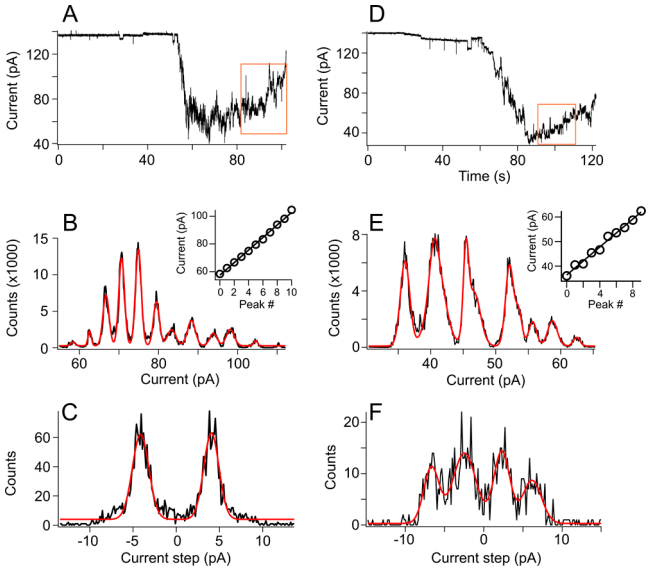

Figure 5. Postexchange step analysis of S-PEG_4 and S-PEG_7 exchange with TP-capped particles. (A–C) S-PEG_4 and (D–F) S-PEG_7 exchanged with TP-capped gold show distinct differences. (A, D) Typical current traces of the before and after exposure of the particles to the ligands. (B, E) All points histograms of the 20 s trace regions highlighted by the orange boxes in (A) and (D) show that the particle fluctuations exhibit transitions between well-defined current states. The insets in (B) and (E) show the peak current positions from the Gaussian mixture fits (solid red line) in both cases. The solid lines in the inset figures are least-squares fits with the following slope parameters s_{PEG7} = 2.8 ± 0.1 pA and s_{PEG4} = 4.2 ± 0.1 pA. The spacing of the S-PEG_4 is in quantitative agreement with the expected value for a homogeneously capped S-PEG_4 gold particle,[20] but the S-PEG_7 is not (i.e., previously established S-PEG_7 current level spacing is 6.49 ± 0.10 pA).[20] (C) S-PEG_4 step distribution shows a single step size δi = −4.12 ± 0.03 pA and δi = 4.06 ± 0.03 pA while (F) the S-PEG_7 step distribution shows multiple steps δi = −2.46 ± 0.09 pA, δi = 2.31 ± 0.08 pA and δi = −6.68 ± 0.10 pA, δi = 6.17 ± 0.14 pA. All data were collected in 3 M KCl at pH 8.0 under a 70 mV applied transmembrane potential. The S-PEG_4 and S-PEG_7 ligand tips contained 540 and 200 μM of free PEG ligands, respectively. Current step distributions shown in (C) and (F) were constructed from 2769 and 983 current step events, respectively, each obtained from four different exchange experiments.

2.5. Single Cluster Ligand Exchange for Peptide Sensing. The ability to monitor ligand exchange on isolated metallic clusters suggests a new method for detecting and characterizing peptides. Rapid and accurate peptide sensing is an active area of research in the nanopore community because nanopore sensors provide a label-free method to detect and identify peptides at the single molecule limit.[43] This makes nanopores ideal because they have the ability to distinguish between several different peptides by using a hand-held device.[44,45]

Previous work has established nanopore sensing for peptides between 1 and 3 kDa, but the technique is less effective for smaller peptides (<1 kDa). This is mostly due to the fact that

https://dx.doi.org/10.1021/acsanm.0c01451
ACS Appl. Nano Mater. 2020, 3, 7973–7981

smaller peptides yield shorter-lived and smaller-magnitude current blockades that make it difficult to accurately identify a given peptide species.[34] This is problematic for a number of peptide sensing applications where small molecular weight peptides are abundant (i.e., cancer diagnostics,[46] antimicrobial peptides,[47] and bioactive peptides[48]). We propose to address this limitation by utilizing rapid ligand exchange to demonstrate low molecular weight peptide sensing.

Figure 6 illustrates the principle of operation, which follows the heterogeneous protocol detailed in Figure 1A. To work as a peptide sensor, this protocol requires a stable initial cluster to undergo rapid exchange with a freely diffusing peptide ligand with a different molecular weight than the exchanged ligand. As an initial proof of concept we used a TP-capped gold cluster as the initial sensor because it yields very stable current states in the α-HL pore. These particles were exposed to the thiol-containing tripeptide glutathione (Gly-Cys-Glu). Monitoring current fluctuations during and after the ligand exchange process allows for the identification of the freely diffusing peptide ligand mass. Figure 6A shows a typical current trace from a single exchange experiment along with the current step distribution during and following exchange. The resulting current step distribution reported in Figure 6C was calculated from nine different cluster exchange experiments. This distribution shows a clearly resolved bimodal function with a small peak centered on the TP ligand step and a larger peak centered on the expected GT ligand step. The known mass of the TP ligands allows us to use the TP peak as a calibrant from which we can measure the mass and corresponding identity of the freely diffusing peptide. In this case the ratio of the peak positions is in quantitative agreement with the ratio of the ligand masses for TP and GT. This demonstrates a rapid and accurate measurement of the freely diffusing peptide. It is worth noting that this analysis was collected with a relatively small number of exchange experiments, which demonstrates an advantage of the exchange protocol where low-molecular-weight peptide markers (<1 kDa) can be rapidly identified in a label-free manner.

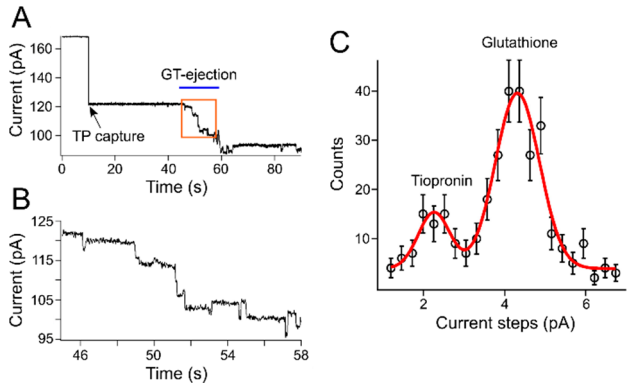

Figure 6. Ligand exchange for single molecule peptide sensing. (A) A typical current trace showing TP-capped gold clusters yield stable currents and ejecting GT tripeptides (highlighted by the blue bar) onto the cluster initiates exchange. After a TP-capped particle is trapped, it remains in the pore until GT is ejected onto the particle for ca. 10 s initiating fluctuations between well-defined current states. (B) The orange box in (A) is highlighted and shows both exchange and addition events (see Figures 4B and 4E). (C) Step current distribution during the exchange process is well fit with a two Gaussian mixture model (red curve) with the small peak centered at 2.26 ± 0.11 pA which corresponds to TP ligands and a larger peak at 4.31 ± 0.04 pA which corresponds to the GT ligands. The ratio of the current steps (r = 1.91 ± 0.09) is in quantitative agreement with the ratio of the ligand masses (r = 1.88) (i.e., m_{TP} = 163.2 Da and m_{GT} = 307.3 Da). The distribution was calculated from 313 current steps collected over nine exchange events on three different α-HL pores. The ejection tip contained 460 μM of free GT. All data were collected under a 70 mV applied transmembrane potential in 3 M KCl at pH 8.

The data shown in Figure 6 correspond to a GT concentration in the peptide ejection tip of 460 μM, which is slightly lower than the known concentration of GT in human cells ($[GT]_{cells} \approx 1$ mM[49]). While this suggests our technique holds promise for the development of a new approach to peptide sensing, several challenges will need to be overcome. A partial list of these includes demonstration of peptide detection within bodily fluids, optimization of ejection tip to pore distance, identification of ideal cluster ligands for peptide exchange, and optimization of experimental conditions (i.e., ionic strength, temperature, applied voltage, etc.). In spite of these issues, our ligand exchange approach to peptide detection provides three major advantages. First, the target cluster can be capped with a known ligand that provides a self-contained calibrant from which one can measure the target peptide. We showed this was possible with the TP-capped clusters, but one can imagine performing peptide measurements with a number of different clusters capped with ligands that have different masses. These could help improve the identification capabilities of the ligand-exchange approach. Second, contrary to most nanopore-based sensing schemes where a single current blockade results from each molecule, our new approach yields numerous fluctuation steps with the addition of each individual peptide. This will lower the limit of detection for our scheme. Finally, the pore dimensions set an upper limit on the size of the peptides that can be detected because peptides larger than 5−7 amino acids in length will not be able to partition into the cluster-containing pore. This will eliminate spurious signal from larger molecules (present in bodily fluids and other biosamples) and enable accurate detection of small, yet biologically relevant peptides.

3. CONCLUSION

Ligand exchange is an important tool for cluster synthesis that enables a variety of applications in many different environments. This report highlights our observations regarding direct manipulation of surface exchange kinetics. Here we focused on thiolate-based ligand exchange and showed how this could be used as a single molecule peptide sensor. However, it is worth noting that nanopore sensing could also be used to study other surface-based effects (i.e., catalysis) or physical characterization (i.e., dipole moments) at the single cluster limit. We believe this report shows the ability to move beyond simple observation of cluster kinetics to direct cluster manipulation, and this strengthens the case for using nanopore sensors as an effective tool for water-soluble metallic cluster analysis and manipulation.

4. METHODS

4.1. Materials. 1,2-Diphytanoyl-*sn*-glycero-3-phosphocholine (DPhy:PC) lipid was purchased from Avanti Polar Lipids (Alabaster, AL). Alpha toxin from *Staphylococcus aureus* was purchased from List Biological Laboratories (Campbell, CA). Teflon partition sheets with preformed 50 μm holes were purchased from Eastern Scientific LLC (Rockville, MD). Borosilicate glass capillaries (with filament) were purchased from Sutter Instruments (Novato, CA). Thiolated PEG_7

https://dx.doi.org/10.1021/acsanm.0c01451
ACS Appl. Nano Mater. 2020, 3, 7973−7981

($S\text{-}PEG_7$) (thiolated PEG with seven repeat ethylene glycol units, MW = 386.5 g/mol) was purchased from Polypure (Oslo, Norway), and thiolated PEG_4 ($S\text{-}PEG_4$) (thiolated PEG with four repeat ethylene glycol units, MW = 224.32 g/mol) was purchased from Quantum Biodesign, Ltd. (Plain City, OH). Ultrapure type I water was obtained from a Direct Q3 filtration system purchased from Millipore-Sigma (Burlington, MA). All other chemical reagents and solvents were purchased from Sigma-Aldrich (St. Louis, MO) and used without further purification unless otherwise stated.

4.2. Cluster Synthesis. Particle synthesis of tiopronin (TP)- and glutathione (GT)-capped gold clusters has been described elsewhere[20] but is briefly summarized here. Synthesis was performed through the reduction of potassium gold(III) chloride ($KAuCl_4$) in the presence of the desired thiolate ligand (TP or GT) using the borane *tert*-butylamine complex (BTBC) as the reducing agent.[50] The synthesis was performed in methanol with molar ratios 1:1:5 mM of gold to ligand to BTBC. The gold salt and ligand solutions were mixed and vigorously shaken for ca. 30 s to form gold−ligand complexes. The BTBC solution was then added and vortexed for 30 s, followed by 20 min of sonication, during which time the solution turned a dark amber color, indicating formation of particles. The solution was then evaporated overnight under atmosphere, leaving behind a black powder. This powder was dissolved in 1 mL of water and set aside at room temperature for experiment. No further size exclusion step was taken because the α-HL nanopore does not yield any signal from particles larger than ca. 3 nm.[51] We have previously shown it is safe to assume the analyzed particles represent a size distribution with low variance, likely of particles ca. 2 nm in diameter.[20]

4.3. Nanopore Sensing. The general methodology used has been described in detail elsewhere,[21] but a brief summary is provided here. Experiments were performed with standard techniques using a single α-HL nanopore sensing channel. A horizontal DPhy:PC bilayer lipid membrane was formed by using a modified painting method[52] in an electrolyte solution (3 M KCl, 10 mM TRIS at pH 8). The membrane spans a 50 μm hole preformed in a 20 μm thick PTFE (Teflon) partition sheet. A single α-HL channel was inserted into the bilayer membrane by using the tip insertion method[21] and confirmed by checking the conductance and comparing this to expected values for a single channel. Similarly, the proper orientation of the pore (*cis* side facing up) was confirmed by comparing current rectification against known values.[53]

Figure 1A and Figure S1 show illustrations of the principle of operation for the experiments described throughout. A 1:4 nanoparticle:electrolyte solution was backloaded into a borosilicate capillary (OD = 1.0 mm and ID = 0.78 mm) formed into a micropipet tip by using preset program #11 on the P-2000 puller (Heat = 350, Fil = 4, Vel = 30, Del = 200) (Sutter Instruments, Novato, CA) with a final ID of 1−2 μm. This nanoparticle-filled micropipet was positioned ca. 50 μm above the membrane and ca. 20 μm to the left edge of the membrane on the *cis*-side of the pore (measured via the MPC-200 controller (Sutter)). A transmembrane voltage was applied (Axopatch 200B, Molecular Devices, Carlsbad, CA) with appropriate polarity (ground held fixed on the *cis*-side of the pore), and a backing pressure of ≈15 hPa was applied through the tip to eject particles (Femtojet, Eppendorf, Hauppauge, NY). The analyte concentration in each tip was 540 μM unless stated otherwise. A rapid downward step in the current indicated the entry of a single cluster into the pore. Single particle insertion is confirmed by the fact that the magnitude of the initial downward step is consistent across all particle captures ($I_{cluster}/I_{open} \approx 0.7$). We propose that only single particle insertion occurs because the GT- and TP-capped particles are anionic in the basic conditions studied herein (pH 8, ligand $pK_a \approx 3-5$[54,55]), and the *cis*-side pore opening is ca. 2.5 nm, which makes entry of multiple particles ($D_{particle} \approx 2$ nm) unlikely. Figure S1 shows homogeneous exchange (i.e., freely diffusing ligands interacting with cluster bound ligands of the same type) is possible in the case where not all the ligands used to synthesize the clusters have been bound to cluster surfaces. In this case, freely diffusing ligands will be ejected near and into the nanopore volume before and during the capture of a single cluster. To remove the freely diffusing ligands, the backing pressure is set to zero over a ca. 1 s period, and this leads to a noticeable change in the cluster-structure dynamics. The other protocol for introducing freely diffusing ligands involves positioning a second tip, identically constructed, near the membrane surface (as viewed with an inverted optical microscope). This is highlighted in Figure 1A where after a cluster is captured the cluster tip is removed and the second tip, which contains the freely diffusing ligand, is positioned near the pore. A backing pressure (ca. 15 hPa) is then applied to the second tip for ≈10 s, and freely diffusing ligands are introduced into the cluster-occupied pore volume. The transmembrane current is continually recorded and used to extrapolate data on possible ligand exchange processes described in the Results section. An upward transition of the current back to the open-pore state indicates the particle exited from the *cis*-side vestibule of the pore in both the homogeneous exchange and heterogeneous exchange experiments. A negative control trace is shown in Figure S4 which highlights the fact that ejecting clean buffer onto a trapped cluster leads to no discernible steps in the current.

4.4. Data Analysis. Data were collected with the Axopatch 200B patch clamp amplifier (Molecular Devices, San Jose, CA) with a 50 kHz sampling frequency and a four-pole 10 kHz low-pass filter. Data analysis was performed with either an IGOR 6.37 (Wavemetrics, Portland, OR) or a MATLAB R2019a (Mathworks, Natick, MA). Postprocessing of data includes digital filtering with a low-pass, four-pole infinite impulse response filter in the IGOR software. An in-house cumulative sum (CUSUM) analyzer was programmed in MATLAB and used to model current steps from which we calculated current step and step time distributions.[20] In some instances, the step distributions where calculated by fitting all points histograms of the different current states with a Gaussian mixture model in IGOR software. All curve fitting, histograms, and digital filtering were performed in IGOR.

Many of the conclusions drawn throughout this article presuppose a linear dependence between ligand mass and current step size. This connection was previously established for $S\text{-}PEG_7$, TP, and 4-mercaptobenzoic acid (4-MBA).[20] We have further expanded the connection between ligand mass and current step size with the addition of $S\text{-}PEG_4$ and GT. Figure S5 shows the linear relationship between the average current step size and the corresponding ligand mass for each of the ligands used throughout this article (i.e., TP, GT, $S\text{-}PEG_4$, and $S\text{-}PEG_7$).

■ ASSOCIATED CONTENT

Supporting Information

The Supporting Information is available free of charge at https://pubs.acs.org/doi/10.1021/acsanm.0c01451.

Schematic illustration of single tip homogeneous exchange and corresponding current trace of $S\text{-}PEG_7$-capped cluster capture in the presence of freely diffusing $S\text{-}PEG_7$, homogeneous ligand exchange and analysis, sample current traces for heterogeneous exchange, blank buffer control and current step/ligand mass calibration curve (PDF)

■ AUTHOR INFORMATION

Corresponding Author

Joseph E. Reiner − *Department of Physics, Virginia Commonwealth University, Richmond, Virginia 23284, United States;* orcid.org/0000-0002-1056-8703; Email: jereiner@vcu.edu

Authors

Bobby D. Cox − *Department of Physics, Virginia Commonwealth University, Richmond, Virginia 23284, United States*

https://dx.doi.org/10.1021/acsanm.0c01451
ACS Appl. Nano Mater. 2020, 3, 7973−7981

Madhav L. Ghimire − *Department of Physics, Virginia Commonwealth University, Richmond, Virginia 23284, United States*

Massimo F. Bertino − *Department of Physics, Virginia Commonwealth University, Richmond, Virginia 23284, United States;* orcid.org/0000-0001-6029-0685

Complete contact information is available at: https://pubs.acs.org/10.1021/acsanm.0c01451

Author Contributions

All authors conceived and designed the experiments. B.D.C. and M.L.G. synthesized clusters and performed nanopore measurements. J.E.R. analyzed data with input from all authors. J.E.R. supervised the project. J.E.R. and B.D.C.wrote the paper with input from all authors.

Funding

This material is based upon work supported by the National Science Foundation under Grant CBET-2011173.

Notes

The authors declare no competing financial interest.

■ ABBREVIATIONS

S-PEG, thiolated poly(ethylene glycol); NMR, nuclear magnetic resonance; MPSA, 3-mercapto-1-propanesulfonate; α-HL, alpha-hemolysin protein; TP, tiopronin; GT, glutathione; DPhy:PC, 1,2-diphytanoyl-*sn*-glycero-3-phosphocholine; BTBC, borane *tert*-butylamine complex; 4-MBA, *p*-mercaptobenzoic acid.

■ REFERENCES

(1) Zhang, Y.; Zhang, C.; Xu, C.; Wang, X.; Liu, C.; Waterhouse, G. I. N.; Wang, Y.; Yin, H. Ultrasmall Au Nanoclusters for Biomedical and Biosensing Applications: A Mini-Review. *Talanta* **2019**, *200*, 432−442.

(2) Liu, M.; Tang, F.; Yang, Z.; Xu, J.; Yang, X. Recent Progress on Gold-Nanocluster-Based Fluorescent Probe for Environmental Analysis and Biological Sensing. *J. Anal. Methods Chem.* **2019**, *2019*, 1.

(3) Layqah, L. A.; Eissa, S. An Electrochemical Immunosensor for the Corona Virus Associated with the Middle East Respiratory Syndrome Using an Array of Gold Nanoparticle-Modified Carbon Electrodes. *Microchim. Acta* **2019**, *186* (4), 224.

(4) Jahangirian, H.; Kalantari, K.; Izadiyan, Z.; Rafiee-Moghaddam, R.; Shameli, K.; Webster, T. J. A Review of Small Molecules and Drug Delivery Applications Using Gold and Iron Nanoparticles. *Int. J. Nanomed.* **2019**, *14*, 1633−1657.

(5) Dinkel, R.; Braunschweig, B.; Peukert, W. Fast and Slow Ligand Exchange at the Surface of Colloidal Gold Nanoparticles. *J. Phys. Chem. C* **2016**, *120* (3), 1673−1682.

(6) Boles, M. A.; Ling, D.; Hyeon, T.; Talapin, D. V. The Surface Science of Nanocrystals. *Nat. Mater.* **2016**, *15* (2), 141−153.

(7) Chen, Y.; Xianyu, Y.; Jiang, X. Surface Modification of Gold Nanoparticles with Small Molecules for Biochemical Analysis. *Acc. Chem. Res.* **2017**, *50* (2), 310−319.

(8) Song, X.-R.; Goswami, N.; Yang, H.-H.; Xie, J. Functionalization of Metal Nanoclusters for Biomedical Applications. *Analyst* **2016**, *141* (11), 3126−3140.

(9) Sels, A.; Salassa, G.; Pollitt, S.; Guglieri, C.; Rupprechter, G.; Barrabés, N.; Bürgi, T. Structural Investigation of the Ligand Exchange Reaction with Rigid Dithiol on Doped (Pt, Pd) Au25 Clusters. *J. Phys. Chem. C* **2017**, *121* (20), 10919−10926.

(10) Huang, Z.; Ishida, Y.; Narita, K.; Yonezawa, T. Kinetics of Cationic-Ligand-Exchange Reactions in Au25 Nanoclusters. *J. Phys. Chem. C* **2018**, *122* (31), 18142−18150.

(11) Ung, T.; Liz-Marzán, L. M.; Mulvaney, P. Controlled Method for Silica Coating of Silver Colloids. Influence of Coating on the Rate of Chemical Reactions. *Langmuir* **1998**, *14* (14), 3740−3748.

(12) Liz-Marzán, L. M.; Giersig, M.; Mulvaney, P. Synthesis of Nanosized Gold−Silica Core−Shell Particles. *Langmuir* **1996**, *12* (18), 4329−4335.

(13) Perez, H.; Pradeau, J.-P.; Albouy, P.-A.; Perez-Omil, J. Synthesis and Characterization of Functionalized Platinum Nanoparticles. *Chem. Mater.* **1999**, *11* (12), 3460−3463.

(14) Luo, Z.; Hou, J.; Menin, L.; Ong, Q. K.; Stellacci, F. Evolution of the Ligand Shell Morphology during Ligand Exchange Reactions on Gold Nanoparticles. *Angew. Chem., Int. Ed.* **2017**, *56* (43), 13521−13525.

(15) Fernando, A.; Aikens, C. M. Deciphering the Ligand Exchange Process on Thiolate Monolayer Protected Au38(SR)24nanoclusters. *J. Phys. Chem. C* **2016**, *120* (27), 14948−14961.

(16) Hossain, S.; Kurashige, W.; Wakayama, S.; Kumar, B.; Nair, L. V.; Niihori, Y.; Negishi, Y. Ligand Exchange Reactions in Thiolate-Protected Au25 Nanoclusters with Selenolates or Tellurolates: Preferential Exchange Sites and Effects on Electronic Structure. *J. Phys. Chem. C* **2016**, *120* (45), 25861−25869.

(17) Fernando, A.; Aikens, C. M. Ligand Exchange Mechanism on Thiolate Monolayer Protected Au25(SR)18 Nanoclusters. *J. Phys. Chem. C* **2015**, *119* (34), 20179−20187.

(18) Hostetler, M. J.; Templeton, A. C.; Murray, R. W. Dynamics of Place-Exchange Reactions on Monolayer-Protected Gold Cluster Molecules. *Langmuir* **1999**, *15* (11), 3782−3789.

(19) Knoppe, S.; Azoulay, R.; Dass, A.; Bürgi, T. In Situ Reaction Monitoring Reveals a Diastereoselective Ligand Exchange Reaction between the Intrinsically Chiral Au38(SR)24 and Chiral Thiols. *J. Am. Chem. Soc.* **2012**, *134* (50), 20302−20305.

(20) Cox, B.; Woodworth, P.; Wilkerson, P.; Bertino, M.; Reiner, J. Ligand-Induced Structural Changes of Thiolate-Capped Gold Nanoclusters Observed with Resistive-Pulse Nanopore Sensing. *J. Am. Chem. Soc.* **2019**, *141* (9), 3792−3796.

(21) Shi, W.; Friedman, A. K.; Baker, L. A. Nanopore Sensing. *Anal. Chem.* **2017**, *89* (1), 157−188.

(22) Yang, J.; Li, S.; Wu, X.-Y.; Long, Y.-T. Development of Biological Nanopore Technique in Non-Gene Sequencing Application. *Chin. J. Anal. Chem.* **2017**, *45* (12), 1766−1775.

(23) Bello, J.; Kim, Y.-R.; Kim, S. M.; Jeon, T.-J.; Shim, J. Lipid Bilayer Membrane Technologies: A Review on Single-Molecule Studies of DNA Sequencing by Using Membrane Nanopores. *Microchim. Acta* **2017**, *184* (7), 1883−1897.

(24) Hasnain, M. J. U.; Afzal, B.; Tehreem Anwar, M. T. P.; Hussain, T. A Review on Nanopore Sequencing Technology, Its Applications and Challenges. *Pure Appl. Biol.* **2020**, *9* (1), 154−161.

(25) Dekker, C. Solid-State Nanopores. *Nat. Nanotechnol.* **2007**, *2* (4), 209−215.

(26) Kasianowicz, J. J.; Robertson, J. W. F.; Chan, E. R.; Reiner, J. E.; Stanford, V. M. Nanoscopic Porous Sensors. *Annu. Rev. Anal. Chem.* **2008**, *1* (1), 737−766.

(27) Reiner, J. E.; Balijepalli, A.; Robertson, J. W. F.; Campbell, J.; Suehle, J.; Kasianowicz, J. J. Disease Detection and Management via Single Nanopore-Based Sensors. *Chem. Rev.* **2012**, *112* (12), 6431−6451.

(28) Branton, D.; Deamer, D. W.; Marziali, A.; Bayley, H.; Benner, S. A.; Butler, T.; Di Ventra, M.; Garaj, S.; Hibbs, A.; Huang, X.; Jovanovich, S. B.; Krstic, P. S.; Lindsay, S.; Ling, X. S.; Mastrangelo, C. H.; Meller, A.; Oliver, J. S.; Pershin, Y. V.; Ramsey, J. M.; Riehn, R.; Soni, G. V.; Tabard-Cossa, V.; Wanunu, M.; Wiggin, M.; Schloss, J. A. The Potential and Challenges of Nanopore Sequencing. *Nat. Biotechnol.* **2008**, *26* (10), 1146−1153.

(29) Campos, E. J.; McVey, C. E.; Astier, Y. Stochastic Detection of MPSA-Gold Nanoparticles Using a α-Hemolysin Nanopore Equipped with a Noncovalent Molecular Adaptor. *Anal. Chem.* **2016**, *88* (12), 6214−6222.

(30) Ettedgui, J.; Kasianowicz, J. J.; Balijepalli, A. Single Molecule Discrimination of Heteropolytungstates and Their Isomers in

Solution with a Nanometer-Scale Pore. *J. Am. Chem. Soc.* **2016**, *138* (23), 7228−7231.
(31) Angevine, C. E.; Chavis, A. E.; Kothalawala, N.; Dass, A.; Reiner, J. E. Enhanced Single Molecule Mass Spectrometry via Charged Metallic Clusters. *Anal. Chem.* **2014**, *86* (22), 11077−11085.
(32) Campos, E. J.; Yates, J. Single Molecule Characterisation of Metal Nanoparticles Using Nanopore-Based Stochastic Detection Methods. *Sens. Actuators, B* **2018**, *255*, 2032−2049.
(33) Cao, C.; Cirauqui, N.; Marcaida, M. J.; Buglakova, E.; Duperrex, A.; Radenovic, A.; Dal Peraro, M. Single-Molecule Sensing of Peptides and Nucleic Acids by Engineered Aerolysin Nanopores. *Nat. Commun.* **2019**, *10* (1), 1−11.
(34) Chavis, A. E.; Brady, K. T.; Hatmaker, G. A.; Angevine, C. E.; Kothalawala, N.; Dass, A.; Robertson, J. W. F.; Reiner, J. E. Single Molecule Nanopore Spectrometry for Peptide Detection. *ACS Sens.* **2017**, *2* (9), 1319−1328.
(35) Robertson, J. W. F.; Reiner, J. E. The Utility of Nanopore Technology for Protein and Peptide Sensing. *Proteomics* **2018**, *18* (18), 1800026.
(36) Agah, S.; Zheng, M.; Pasquali, M.; Kolomeisky, A. B. DNA Sequencing by Nanopores: Advances and Challenges. *J. Phys. D: Appl. Phys.* **2016**, *49* (41), 413001.
(37) Wu, H.-C.; Bayley, H. Single-Molecule Detection of Nitrogen Mustards by Covalent Reaction within a Protein Nanopore. *J. Am. Chem. Soc.* **2008**, *130* (21), 6813−6819.
(38) Harrington, L.; Alexander, L. T.; Knapp, S.; Bayley, H. Pim Kinase Inhibitors Evaluated with a Single-Molecule Engineered Nanopore Sensor. *Angew. Chem., Int. Ed.* **2015**, *54* (28), 8154−8159.
(39) Zhao, Q.; Jayawardhana, D. A.; Wang, D.; Guan, X. Study of Peptide Transport through Engineered Protein Channels. *J. Phys. Chem. B* **2009**, *113* (11), 3572−3578.
(40) Dahan, I.; Sorrentino, S.; Boujemaa-Paterski, R.; Medalia, O. Tiopronin-Protected Gold Nanoparticles as a Potential Marker for Cryo-EM and Tomography. *Structure* **2018**, *26* (10), 1408.
(41) Ansar, S. M.; Mohammed, F. S.; von White, G.; Budi, M.; Powell, K. C.; Mefford, O. T.; Kitchens, C. L. Effect of Postsynthesis Purifications on Gold and Silver Nanoparticle Ligand Coverage. *J. Phys. Chem. C* **2016**, *120* (12), 6842−6850.
(42) Raillon, C.; Granjon, P.; Graf, M.; Steinbock, L. J.; Radenovic, A. Fast and Automatic Processing of Multi-Level Events in Nanopore Translocation Experiments. *Nanoscale* **2012**, *4* (16), 4916−4924.
(43) Lin, Y.; Ying, Y.-L.; Shi, X.; Liu, S.-C.; Long, Y.-T. Direct Sensing of Cancer Biomarkers in Clinical Samples with a Designed Nanopore. *Chem. Commun.* **2017**, *53* (84), 11564−11567.
(44) Izawa, Y.; Osaki, T.; Kamiya, K.; Fujii, S.; Misawa, N.; Miki, N.; Takeuchi, S. Handheld Nanopore-Based Biosensing Device. *2018 IEEE Micro Electro Mechanical Systems (MEMS)* **2018**, 2−5.
(45) Morin, T. J.; McKenna, W. L.; Shropshire, T. D.; Wride, D. A.; Deschamps, J. D.; Liu, X.; Stamm, R.; Wang, H.; Dunbar, W. B. A Handheld Platform for Target Protein Detection and Quantification Using Disposable Nanopore Strips. *Sci. Rep.* **2018**, *8* (1), 1−12.
(46) Bhalla, S.; Verma, R.; Kaur, H.; Kumar, R.; Usmani, S. S.; Sharma, S.; Raghava, G. P. S. CancerPDF: A Repository of Cancer-Associated Peptidome Found in Human Biofluids. *Sci. Rep.* **2017**, *7* (1), 1511.
(47) Wang, G.; Li, X.; Wang, Z. APD3: The Antimicrobial Peptide Database as a Tool for Research and Education. *Nucleic Acids Res.* **2016**, *44* (D1), D1087−D1093.
(48) Agyei, D.; Pan, S.; Acquah, C.; Bekhit, A. E.-D. A.; Danquah, M. K. Structure-Informed Detection and Quantification of Peptides in Food and Biological Fluids. *J. Food Biochem.* **2019**, *43* (1), e12482.
(49) Forman, H. J.; Zhang, H.; Rinna, A. Glutathione: Overview of Its Protective Roles, Measurement, and Biosynthesis. *Mol. Aspects Med.* **2009**, *30* (1), 1−12.
(50) Bertino, M. F.; Sun, Z.-M.; Zhang, R.; Wang, L.-S. Facile Syntheses of Monodisperse Ultrasmall Au Clusters. *J. Phys. Chem. B* **2006**, *110* (43), 21416−21418.
(51) Song, L.; Hobaugh, M. R.; Shustak, C.; Cheley, S.; Bayley, H.; Gouaux, J. E. Structure of Staphylococcal α-Hemolysin, a Heptameric Transmembrane Pore. *Science* **1996**, *274* (5294), 1859.
(52) Angevine, C. E.; Seashols-Williams, S. J.; Reiner, J. E. Infrared Laser Heating Applied to Nanopore Sensing for DNA Duplex Analysis. *Anal. Chem.* **2016**, *88* (5), 2645−2651.
(53) Bhattacharya, S.; Muzard, J.; Payet, L.; Mathé, J.; Bockelmann, U.; Aksimentiev, A.; Viasnoff, V. Rectification of the Current in α-Hemolysin Pore Depends on the Cation Type: The Alkali Series Probed by Molecular Dynamics Simulations and Experiments. *J. Phys. Chem. C* **2011**, *115* (10), 4255−4264.
(54) Templeton, A. C.; Chen, S.; Gross, S. M.; Murray, R. W. Water-Soluble, Isolable Gold Clusters Protected by Tiopronin and Coenzyme A Monolayers. *Langmuir* **1999**, *15* (1), 66−76.
(55) Dawson, R. M. C.; Elliott, D. C.; Elliott, W. H.; Jones, K. M. *Data for Biochemical Research*, 3rd ed.; Oxford Science Publications: Oxford, 1986; p 580.

https://dx.doi.org/10.1021/acsanm.0c01451
ACS Appl. Nano Mater. 2020, 3, 7973−7981